Journal of Catalysis **199,** 171–176 (2001)
doi:10.1006/jcat.2000.3147, available online at http://www.idealibrary.com on IDEAL®

The NO + CO Reaction Catalyzed by Flat, Stepped, and Edged Pd Surfaces

B. Hammer[1]

Institute of Physics and Astronomy, University of Aarhus, DK-8000 Aarhus C, Denmark

Received June 26, 2000; revised November 14, 2000; accepted November 16, 2000; published online March 21, 2001

The catalytic reduction of NO by CO at Pd surfaces is studied using density functional theory. The reaction pathways and energy barriers of the elementary reaction steps are calculated at four different Pd surfaces: Pd(111), Pd(100), stepped Pd(211), and edged, missing-row reconstructed Pd(311). The stability of the reaction intermediates, chemisorbed NO, CO, N_2, N, and O, varies only moderately with the Pd surface structure. The energy barriers for the elementary reaction steps vary, however, more strongly with the Pd structure. The energy barriers for NO dissociation and for N_2 association are found to be much smaller at palladium steps and edges compared to the values at flat Pd(111) and Pd(100). For the CO_2 formation, steps and edges have little influence on the energy barrier, reflecting that the flat Pd(100) surface already contains a very favorable ensemble for the CO_2 formation.

Key Words: **palladium; metal surface; chemisorption; reactivity; defects; NO reduction; CO oxidation; three-way catalyst.**

1. INTRODUCTION

Catalytic conversion of automotive exhaust gas is an important issue in keeping emissions of environmental pollutants from modern motor vehicles low. Exhaust gas, for example, contains toxic nitrogen oxides, NO_x (e.g., NO and NO_2), that are produced thermally through a gas-phase reaction of N_2 and O_2 at the elevated temperatures in combustion engines. Other pollutants in exhaust gas are CO and unburned hydrocarbons. To eliminate the emission of these pollutants three-way catalysts (TWC) have been developed. TWCs serve three purposes: simultaneous reduction of NO_x, oxidation of CO, and combustion of the hydrocarbons. TWCs have typically been based on small Rh + Pt particles as the active component, but since the early 1990s, a TWC based on Pd particles has been used in the United States (1, 2).

The CO is greatly in excess of, e.g., the NO in the untreated exhaust gas. CO may therefore serve as the reducing agent for the NO reduction. While the overall reaction of NO + CO over a TWC is well known, no complete microscopic description of the catalytic steps has been provided so far. Further, despite many single crystalline studies of molecular reactions, the role of the Pd surface structure is not yet understood.

In the present paper we aim at providing considerable insight into the NO + CO reaction using the modern quantum mechanical computational method: density functional theory (DFT). In order to allow for a discussion of the structure sensitivity of the reaction, the NO + CO reaction will be studied at four different surface structures of palladium. The individual reaction steps will be investigated with the aim of identifying the relevant reaction intermediates at the catalytic surface. The full DFT potential energy diagram for the reaction is presented and the important reactive surface sites are determined.

2. RESULTS

Adjusting for stoichiometry, the full NO + CO gas-phase reaction is

$$2NO + 2CO \rightarrow N_2 + 2CO_2.$$

When a catalytic surface is introduced, the reaction may be considered as having the following elementary steps:

$$NO \rightarrow NO_a \quad \text{[Ia]}$$
$$CO \rightarrow CO_a \quad \text{[Ib]}$$
$$NO_a \rightarrow N_a + O_a \quad \text{[Ic]}$$
$$CO_a + O_a \rightarrow CO_2 \quad \text{[Id]}$$
$$2N_a \rightarrow N_{2,a} \quad \text{[IIa]}$$
$$N_{2,a} \rightarrow N_2, \quad \text{[IIb]}$$

where the reactions Ia–d need to occur twice for every time the reactions IIa,b take place. To model the NO + CO reaction at a palladium catalyst we therefore need to study individual molecular adsorption/desorption and dissociation/association events and to investigate the stability of the atomic reaction intermediates, N_a and O_a. We will do so at low surface coverage corresponding to the situation at a high reaction temperature.

[1] E-mail: hammer@ifa.au.dk.

0021-9517/01 $35.00

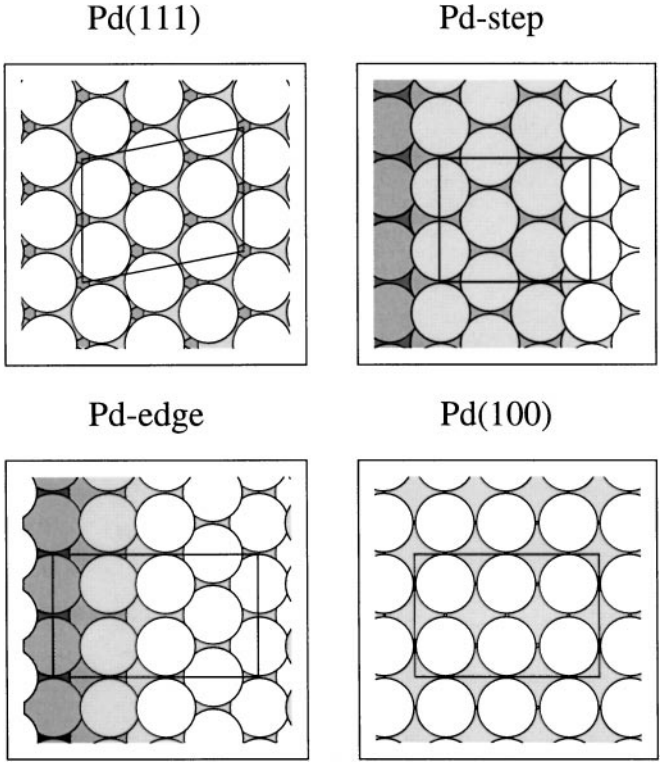

FIG. 1. Top view illustrations of the slabs used for the computations. In the case of Pd-step and Pd-edge, the Pd atoms (spheres) have been shaded to highlight the close-packed facets.

2.1. *Calculational Setup*

Palladium slabs with surface unit cells, Pd(111)-c(6×2), Pd(211)-p(2×1), Pd(311)-c(2×4)-missing-row, and Pd(100)-p(2×3), constitute our models for Pd(111), monatomic Pd steps, Pd edges, and Pd(100), respectively. The surface unit cells are illustrated in Fig. 1. The number of Pd layers in each slab system is chosen so that the supercell contains a total of 24 Pd atoms. The slabs describing Pd(111), Pd-step, and Pd(100) that expose six Pd atoms in the surface thereby have four Pd layers while the Pd-edge slab has three Pd layers (in the studies of O_a relative to $\frac{1}{2}O_2$ we use, however, four layers). The bottom-most two Pd layers are held fixed at the truncated bulk positions while all other ionic degrees of freedom are fully relaxed. Transition states are localized by relaxing the systems with one intramolecular bond length fixed at a series of elongated values (1.7 Å, 2.0 Å, 2.3 Å, and larger where necessary).

The ionic cores are described by ultrasoft pseudopotentials (3) (with core cutoff radii: $r_c^C = r_c^N = 0.6$ bohr, $r_c^O = 0.7$ bohr, and $r_c^{Pd} = 1.1$ bohr) and the Kohn–Sham one-electron valence states are expanded in a basis of plane waves with kinetic energies below 25 Ry at uniform (4×4) (or (6×4) in the studies of O_a relative to $\frac{1}{2}O_2$) **k**-point sampling meshes within the first surface Brillouin zone for all four surface unit cells. The calculations are self-consistent within the GGA-PW91 exchange-correlation (XC) description (4). This also applies in the pseudopotential construction and in the evaluation of the theoretical Pd lattice constant, $a = 3.985$ Å. For the reaction energies and energy barriers, we report GGA-PW91 results only as a reference to the literature. Rather, we focus on results for the reaction energetics as calculated non-self-consistently using the GGA-RPBE functional (5). The RPBE functional is a GGA functional with a greatly improved description of molecular bond energies (6). With the present calculational method we obtain GGA-RPBE-based molecular bond energies of 6.75, 10.84, 9.84, 5.51, and 16.80 eV for NO, CO, N_2, O_2, and CO_2, respectively (7). The corresponding experimental values (excluding zero-point energy contributions) are 6.63, 11.24, 9.91, 5.22, and 16.87 eV (8). Despite the improvements in the XC description using the GGA-RPBE functional there are thus calculational errors of up to 0.4 eV in the molecular bond energies. These errors will inevitably be carried over to the calculated reaction energetics. When, however, focus is put on *changes* in the reaction energetics from one surface to the next as in the discussion of the structure sensitivity in the present paper, error cancellation means that the discussion of smaller energy differences becomes meaningful.

We note that while the reduction of NO at Ru, Rh, and Pd surfaces (9–11) and the oxidation of CO at Ru and Pt surfaces (12–14) have previously been subject to individual studies by DFT slab methods, the present paper is the first to report the complete DFT reaction diagram for the NO + CO reaction at a metal surface described by the reliable slab approach.

2.2. *Adsorption/Desorption*

We first consider the adsorption/desorption of NO, CO, N_2, N, and O. The chemisorption configurations are depicted in Fig. 2 where also the reaction energies are given. Table 1 further contains the reaction energies for the reaction steps Ia,b and IIb. For the molecularly adsorbed species, NO_a, CO_a, and $N_{2,a}$, we find configurations at the Pd-step and Pd-edge that are favored over configurations at the Pd(111) and Pd(100). The effect of stronger bonding at step and edge sites has been explained as caused by the lower coordination of the step and edge Pd atoms leading to higher reactivity of these Pd atoms (15). The higher reactivity may be quantified in terms of the energetic position of the Pd 4*d*-electrons which is generally found to be higher at the low-coordinated sites (11, 16–18).

The $N_{2,a}$ is bound atop a Pd atom at all surfaces considered. The comparison of the bonding at Pd(111) and Pd(100) with the bonding at Pd-step and Pd-edge is therefore particularly simple for this species. $N_{2,a}$ is about 0.2 eV more strongly bound at Pd-step and Pd-edge sites, suggesting this to be the scale for the effect of the lower Pd–Pd

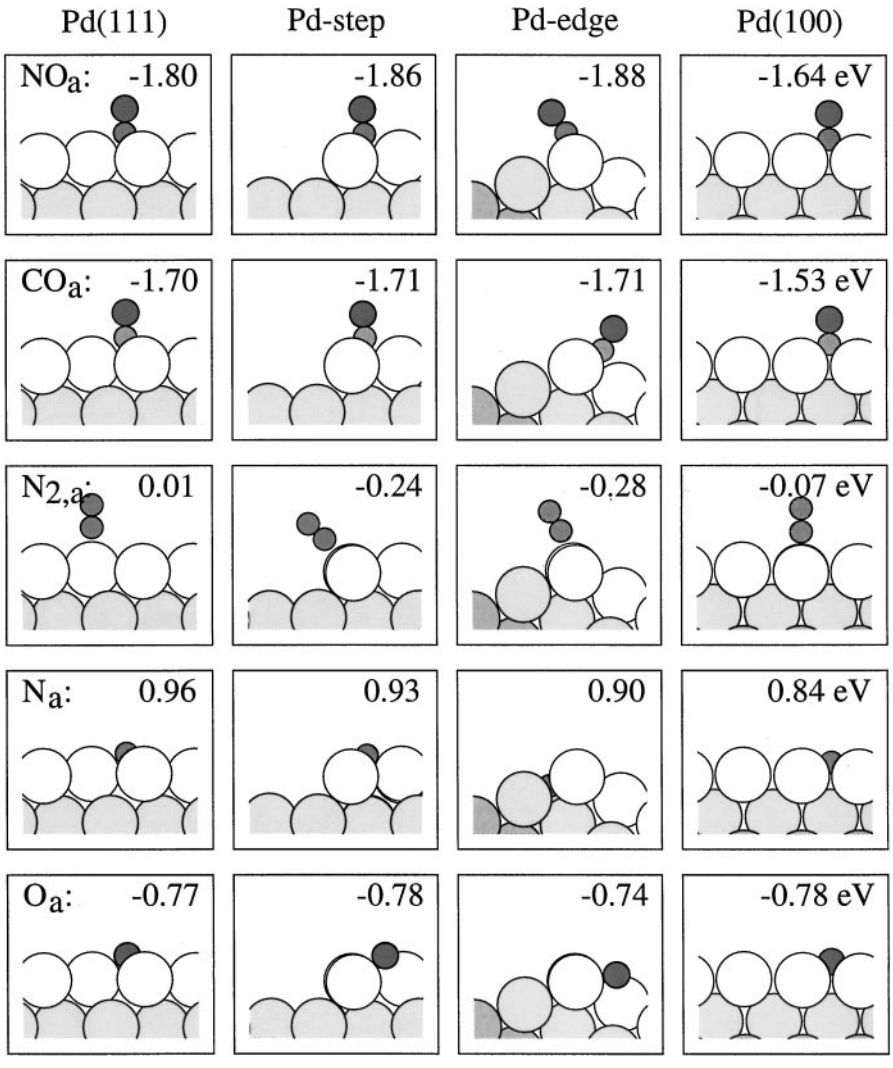

FIG. 2. Chemisorption configurations for molecular NO_a, CO_a, and $N_{2,a}$ and atomic N_a and O_a at the four Pd surfaces considered. The GGA-RPBE chemisorption reaction energies (in electronvolts, negative values indicating exothermicity) are relative to NO, CO, N_2, $\frac{1}{2}N_2$, and $\frac{1}{2}O_2$, respectively.

coordination at such defects. NO_a and CO_a that are more highly coordinated at Pd(111) and Pd(100) probe less of the effect of the higher reactivity at Pd-step and Pd-edge because (i) these molecules either keep their high coordination at the defect (e.g., NO/Pd-step) and hence do not coordinate solely to highly reactive Pd atoms or (ii) they move to a lower coordination site (e.g., NO/Pd-edge) whereby they manage to coordinate solely to highly reactive Pd atoms at the expense, however, of losing some of the bonding associated with the high coordination.

For the atomic adsorbates, N_a and O_a, the high coordination is associated with a large energy gain. These adsorbates therefore remain in high-coordination sites and the effect of the higher reactivity of the Pd-step and Pd-edge atoms is only reflected to a small degree, as in the case of the NO_a and CO_a. For O_a at the Pd-edge, the effect even appears to be reversed. A most interesting observation can be made: the four-fold coordination of N_a at Pd(100) is favored over N_a at any of the other surfaces. Similar reports have been made for N_a at Fe surfaces (19) and it appears to be a general phenomenon.

2.3. *Dissociation/Association Reactions*

We now turn to the dissociation of NO_a and the association of CO_a and O_a to CO_2 and of $2N_a$ to $N_{2,a}$. The dissociation of CO_a is further considered as this allows for an assessment of the possible role of such a side reaction. The calculated transition states are depicted in Fig. 3 where also the energy barriers are given. The reaction energies and the energy barriers for reaction steps Ic,d and IIa are further given in Table 1. For the diatomic reactions, NO_a and CO_a dissociation and $2N_a$ association, the monoatomic Pd steps are seen to give rise to the lowest reaction barriers among

TABLE 1

Reaction Energies and Energy Barriers (in eV) for the Individual Reaction Steps Evaluated with the GGA-RPBE (Boldface) or GGA-PW91 Functional[a]

	Reaction	XC	Reaction energy				Energy barrier			
			Pd(111)	Pd-step	Pd-edge	Pd(100)	Pd(111)	Pd-step	Pd-edge	Pd(100)
[Ia]	$NO \rightarrow NO_a$	GGA-RPBE	**−1.80**	**−1.86**	**−1.88**	**−1.64**	—	—	—	—
		GGA-PW91	−2.29	−2.31	−2.34	−2.17				
[Ib]	$CO \rightarrow CO_a$	GGA-RPBE	**−1.70**	**−1.71**	**−1.71**	**−1.53**	—	—	—	—
		GGA-PW91	−2.18	−2.15	−2.19	−2.02				
[Ic]	$NO_a \rightarrow N_a + O_a$	GGA-RPBE	**1.03**	**1.09**	**1.10**	**0.79**	**2.7**	**1.9**	**2.3**	**2.3**
		GGA-PW91	0.81	0.89	0.80	0.56	2.6	1.6	2.1	2.1
[Id]	$CO_a + O_a \rightarrow CO_2$	GGA-RPBE	**−0.70**	**−0.74**	**−0.75**	**−0.92**	**1.4**	**1.0**	**0.7**	**0.7**
		GGA-PW91	−0.08	−0.16	−0.13	−0.27	1.4	1.0	0.8	0.8
[IIa]	$2N_a \rightarrow N_{2,a}$	GGA-RPBE	**−1.91**	**−2.10**	**−2.08**	**−1.75**	**2.0**	**1.3**	**1.8**	**2.1**
		GGA-PW91	−1.49	−1.73	−1.52	−1.29	2.1	1.3	2.1	2.2
[IIb]	$N_{2,a} \rightarrow N_2$	GGA-RPBE	**−0.01**	**0.24**	**0.28**	**0.07**	—	—	—	—
		GGA-PW91	0.30	0.53	0.59	0.40				

[a]According to previous studies, the GGA-RPBE functional appears to give the most accurate description of intramolecular and molecule–surface bonding (5, 6).

the surfaces considered. This is due to a particularly stable reaction ensemble present at the step as reported previously for NO and N_2 dissociation at stepped Ru(0001) surfaces (9, 20). In this reaction configuration one end of the diatomic molecule is bound to Pd atoms at the base of the step while the other end is bound to the highly reactive Pd atoms in the step. It is mainly the high coordination of the reacting diatomic molecule to the surface which is responsible for the favorable barrier at this reaction configuration (9).

The Pd-edge is also found to give favorable reaction sites for the diatomics, although the effect is smaller than for the Pd-step in particular when comparing to the Pd(100) surface. The Pd(111) surface which is the most compact of the surfaces considered is clearly the least reactive surface for dissociation/association of the diatomic molecules. Irrespective of the surface considered, the energy barrier for CO_a dissociation is found to be exceedingly large (more than 3 eV) and this side reaction can therefore be disregarded.

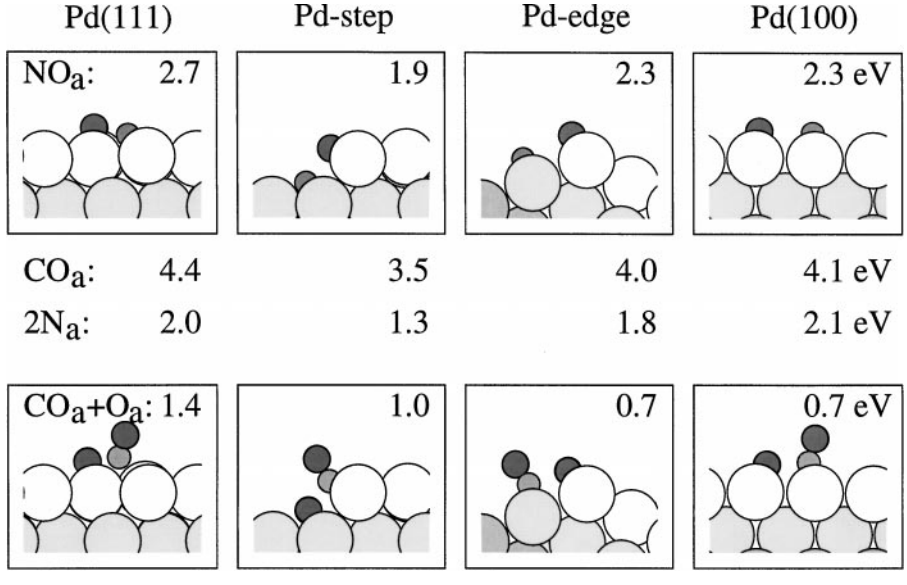

FIG. 3. Transition states (TS) for the $NO_a \rightarrow N_a + O_a$ and the $CO_a + O_a \rightarrow CO_2$ reactions at the four Pd surfaces. The GGA-RPBE energy barriers with respect to NO_a and $CO_a + O_a$ are given in electronvolts. The TSs for the $CO_a \rightarrow C_a + O_a$ and the $2N_a \rightarrow N_{2,a}$ reactions are very similar to the depicted NO_a dissociation TS and are therefore not shown. Given are, however, the energy barriers for these reactions with respect to CO_a and $2N_a$, respectively.

Moving to the CO_2 formation reaction we note that also for this reaction the Pd(111) provides the least favorable pathway with a high energy barrier. This barrier is lowered considerably at the Pd-step and Pd-edge sites, but unlike for the diatomic reactions, the Pd-edge is the most favorable of the two sites. The CO_2 formation at the Pd(100) surface is subject to an energy barrier similar to that at the Pd-edge, i.e., a rather small barrier. In fact, the transition states at the Pd(100) and Pd-edge are very similar and it appears that the main effect of the Pd-edge is to expose a small Pd(100) facet. Returning to the diatomic reactions, a comparison of the transition states at Pd(100) and Pd-edge leads to a similar conclusion.

3. DISCUSSION

We are now in position to construct the full reaction diagram for the NO + CO reaction. This is done in Fig. 4, where the calculated reaction energies and energy barriers for the reactions Ia–d and IIa,b are shown in succession for a surface already hosting N_a. The preadsorbed N_a is assumed to originate from reaction steps Ia–d and the potential energy curves in the figure therefore start at the reaction energy of steps Ia–d (about −3.2 eV, depending on the Pd surface considered). All four potential energy curves (one for each Pd surface) end up at the same value, −8.28 eV, which is our calculated reaction energy of the gas-phase reaction $2NO + 2CO \rightarrow N_2 + 2CO_2$ independent of the structure of the catalytic palladium surface.

Comparing the potential energy curves for the different Pd surfaces, it is seen from Fig. 4 how the variations in the stability of the reaction intermediates, NO_a, CO_a, N_a, O_a, and $N_{2,a}$, are generally small compared to the variations in the energy barriers for the elementary reaction steps, NO dissociation, and CO_2 and N_2 formation. The kinetics of the NO + CO reaction may therefore be discussed mainly on the basis of the energy barriers. It is evident from the figure that the reaction is predicted to run faster on Pd surfaces with steps and edges than on Pd(111) and Pd(100). In particular, the NO dissociation and the N_2 formation are associated with large energy barriers and therefore appear to be inhibiting for the rate in the absence of Pd steps and to some degree of Pd-edge sites.

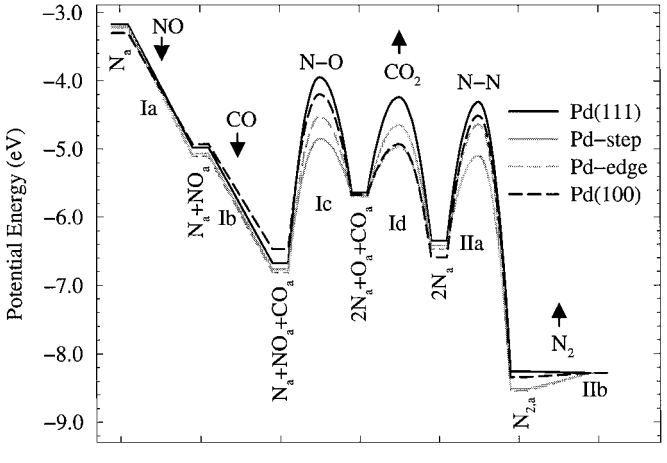

FIG. 4. Energy diagram showing GGA-RPBE potential energies for the NO + CO reaction at four N_a precovered Pd surfaces. NO and CO adsorption, Ia,b, is followed by NO_a dissociation, Ic, CO_2 formation, Id, $N_{2,a}$ association, IIa, and finally $N_{2,a}$ desorption, IIb.

Focusing on the NO dissociation, we can quantify this finding further. The NO dissociation barrier at the Pd-step is favored by at least 0.4 eV over reaction at any of the other surfaces (cf. Fig. 3). This means that, e.g., at 500 K, the steps will be about 10^5 times more reactive per site than the other surfaces. Tiny amounts of Pd-steps on otherwise flat Pd surfaces may therefore completely dominate the kinetics of the NO + CO reaction.

3.1. Summary of Experimental Results

The NO + CO reaction on palladium has been studied experimentally in great detail. The palladium samples studied include monocrystaline Pd (21, 22), Pd clusters grown on flat supports, e.g., Pd/α-Al_2O_3(0001) (21, 23, 24) and Pd/MgO(100) (25, 26), and high-surface-area Pd clusters prepared by washcoating or other techniques (21, 27). The general finding is that Pd catalyzes the CO oxidation to CO_2 and the NO reduction to N_2 with only small yields of side reactions (e.g., N_2O formation).

The NO dissociation is reported to be the rate-limiting step at low temperature while the CO adsorption is rate limiting at high temperature (26). The Pd(111) is found to be more reactive than Pd(100) for the steady-state NO + CO reaction, which is explained as being due to inactive N_a forming on Pd(100) (21, 24, 26). Some controversy exists for the reactivity dependence on cluster size. Rainer *et al.* report large clusters are more reactive than small clusters (21, 24), while Piccolo and Henry demonstrate that small or medium-sized (∼70 Å) clusters are the more reactive (25, 26). "Reverse spill-over" of physisorbed NO or CO from the support only taken into account by Piccolo and Henry (25, 26) appears to explain the apparent controversy.

Temperature-programmed desorption (TPD) of NO_a at Pd(211) yields in addition to NO also N_2 and N_2O (28, 29). At Pd(111) TPD of NO_a exclusively gives NO desorption. This reveals that NO dissociation is facilitated by the Pd steps at Pd(211) which has (111) terraces and (100) steps, compared to the situation at "flat" Pd(111) (28). TPD of $NO_a + CO_a$ at Pd(320), which has (110) facets and (100) steps, produces N_2 and CO_2 in large amounts which further demonstrates that the NO reduction by CO is favored by steps.

3.2. Comparison of Theory and Experiment

The present theoretical findings that palladium steps are highly reactive are in good accord with the experimental

observations of enhanced reactivity of stepped Pd(211) (28, 29) and Pd(320) surfaces (22) and of small and medium-sized clusters when corrected for "reverse spill-over" (25, 26). The observation that Pd(111) is more reactive than Pd(100) is less obviously in accord with the present results, but several facts are likely to explain this. First, the Pd-steps considered in the present work are only present at Pd(111) facets. The geometry of monatomic steps is different at Pd(100). As the high reactivity of the Pd(111)-steps is intimately related to the high coordination of a transition-state complex possible at this step geometry (9), a similar high reactivity of Pd(100)-steps cannot be expected *a priori*. Second, as noted above, the N_a is more stable at Pd(100) than at Pd(111) and reaction at Pd(100) may well be hampered by N_a to a larger degree than reaction at Pd(111). The energy difference between N/Pd(100) and N/Pd(111) is, however, small. Finally, O_a may also prove to be influencing the experimental work and hence the conclusions with respect to relative reactivity of the different facets of Pd clusters. Oxygen is known to dissolve into the bulk at 550 K in single crystalline studies (28), but dealing with small Pd clusters, the oxidation state of the Pd surfaces is yet a matter of debate (27).

4. CONCLUSION

In summary, we have calculated the complete reaction potential energy diagram for $NO + CO$ at four different Pd surfaces. Monoatomic steps at Pd(111) are found to represent the most reactive sites for the NO dissociation and the N_2 formation, while Pd(100) and Pd-edge are the most reactive for the CO_2 formation.

ACKNOWLEDGMENTS

Discussions with J. K. Nørskov and I. Stensgaard are gratefully acknowledged. This work was supported by The Danish Research Councils (Grants No. 9800425 and No. 9803041).

REFERENCES

1. Shelef, M., and Graham, G. W., *Catal. Rev. Sci. Eng*. **36**, 433 (1994).
2. Nieuwenhuys, B. E., *Adv. Catal*. **44**, 259 (2000).
3. Vanderbilt, D. H., *Phys. Rev. B* **41**, 7892 (1990).
4. Perdew, J. P., Chevary, J. A., Vosko, S. H., Jackson, K. A., Pederson, M. R., Singh, D. J., and Fiolhais, C., *Phys. Rev. B* **46**, 6671 (1992).
5. Hammer, B., Hansen, L. B., and Nørskov, J. K., *Phys. Rev. B* **59**, 7413 (1999).
6. Kurth, S., Perdew, J. P., and Blaha, P., *Int. J. Quantum Chem*.**75**, 889 (1999).
7. The corresponding GGA-PW91 values are 7.01, 11.24, 10.04, 5.84, and 17.55 eV for NO, CO, N_2, O_2, and CO_2, respectively.
8. Pople, J. A., Head-Gordon, M., Fox, D. J., Raghavachari, K., and Curtiss, L. A., *J. Chem. Phys*. **90**, 5622 (1989); Curtiss, L. A., Jones, C., Trucks, G. W., Raghavachari, K., and Pople, J. A., *J. Chem. Phys*. **93**, 2537 (1990).
9. Hammer, B., *Phys. Rev. Lett*. **83**, 3681 (1999); *Surf. Sci*. **459**, 323 (2000).
10. Loffreda, D., Simon, D., and Sautet, P., *J. Chem. Phys*. **108**, 6447 (1998).
11. Hammer, B., *Faraday Discuss*. **110**, 323 (1998).
12. Stampfl, C., and Scheffler, M., *Phys. Rev. Lett*. **78**, 1500 (1997).
13. Alavi, A., Hu, P., Deutsch, T., Silvestrelli, P. L., and Hutter, J., *Phys. Rev. Lett*. **80**, 3650 (1998).
14. Eichler, A., and Hafner, J., *Phys. Rev. B* **59**, 5960 (1999).
15. Yates, J. T., Jr., *J. Vac. Sci. Technol. A* **13**, 1359 (1995).
16. Hammer, B., Nielsen, O. H., and Nørskov, J. K., *Catal. Lett*. **46**, 31 (1997).
17. Hammer, B., and Nørskov, J. K., *Phys. Rev. Lett*. **79**, 4441 (1997).
18. Hammer, B., and Nørskov, J. K., *Adv. Catal*. **45**, 71 (2000).
19. Mortensen, J. J., Hansen, L. B., Hammer, B., and Nørskov, J. K., *J. Catal*. **182**, 479 (1999).
20. Dahl, S., Logadottir, A., Egeberg, R. C., Larsen, J. H., Chorkendorff, I., Törnqvist, E., and Nørskov, J. K., *Phys. Rev. Lett*. **83**, 1814 (1999).
21. Rainer, D. R., Vesecky, S. M., Koranne, M., Oh, W. S., and Goodman, D. W., *J. Catal*. **167**, 234 (1997).
22. Hirsimäki, M., Suhonen, S., Pere, J., Valden, M., and Pessa, M., *Surf. Sci*. **402–404**, 187 (1998).
23. Cordatos, H., Bunluesin, T., and Gorte, R. J., *Surf. Sci*. **323**, 219 (1995).
24. Rainer, D. R., Koranne, M., Vesecky, S. M., and Goodman, D. W., *J. Phys. Chem. B* **101**, 10769 (1997).
25. Piccolo, L., and Henry, C. R., *Appl. Surf. Sci*. **162**, 670 (2000).
26. Piccolo, L., and Henry, C. R., *J. Mol. Catal. A* **167**, 181 (2001).
27. Almusaiteer, K., and Chung, S. S. C., *J. Catal*. **184**, 189 (1999).
28. Ramsier, R. D., Gao, Q., Neergaard, H., Lee, K.-W., Nooij, O. W., Lefferts, L., and Yates, J. T., Jr., *Surf. Sci*. **320**, 209 (1994).
29. Ikai, M., and Tanaka, K., *J. Chem. Phys*. **110**, 7031 (1999).